hiPSC-derived astrocytes from individuals with schizophrenia induce a dystrophic phenotype in microglial-like cells

Pablo L. Cardozo[1], Chia-Yi Lee[2,#], Juliana P. S. Lacerda[1,#], Júlia S. Fahel[1], Pablo Trindade[3,10], Gabriela Vitória[3], Leonardo Chicaybam[4,5], Rafaela C. Cordeiro[1], Isaque J. S. de Faria[1], Nathália C. Silva[1], Yaovi M. H. Todjro[1], Joana C. do P. Maciel[3], Martin H. Bonamino[4,5], Luciene B. Vieira[6], Breno F. Cruz[7], Rodrigo Nicolato[7], Kristen J. Brennand[2,8], Stevens K. Rehen[3,9], Fabíola M Ribeiro[1,*]

1- Department of Biochemistry and Immunology, Institute of Biological Sciences (ICB), Universidade Federal de Minas Gerais (UFMG), Belo Horizonte, MG, Brazil; 2- Department of Genetics, Yale School of Medicine, Yale University, New Haven, CT, United States of America; 3- D'or Institute for Research and Education (IDOR), Rio de Janeiro, RJ, Brazil; 4- Molecular Carcinogenesis Program, Research Coordination, Instituto Nacional do Câncer (INCA), Rio de Janeiro, RJ, Brazil; 5- Vice-Presidency of Research and Biological Collections (VPPCB), Fundação Oswaldo Cruz (FIOCRUZ), Rio de Janeiro, RJ, Brazil; 6- Department of Pharmacology, Institute of Biological Sciences (ICB), Universidade Federal de Minas Gerais (UFMG), Belo Horizonte, MG, Brazil; 7- Department of Psychiatry, Faculty of Medicine, Universidade Federal de Minas Gerais (UFMG), Belo Horizonte, MG, Brazil; 8- Department of Psychiatry, Yale School of Medicine, Yale University, New Haven, CT, United States of America; 9- Department of Genetics, Institute of Biology, Universidade Federal do Rio de Janeiro (UFRJ), Rio de Janeiro, RJ, Brazil; 10- Current affiliation: Department of Clinical Analysis and Toxicology, Faculty of Pharmacy, Universidade Federal do Rio de Janeiro (UFRJ), Rio de Janeiro, RJ, Brazil

* Corresponding author: fmribeiro@icb.ufmg.br

[#] These authors contributed equally to this work.

Running title: SCZ astrocytes induce dystrophic microglia

Keywords: schizophrenia; astrocytes; microglia; dystrophic; senescence; CX3CL1

ABSTRACT

Background: Neuroinflammation, particularly astrocyte reactivity, is increasingly linked to schizophrenia (SCZ). Yet, the crosstalk between astrocytes and microglia in SCZ, especially under pro-inflammatory conditions, remains unclear.

Methods: Here, we employed human induced-pluripotent stem cells to compare how astrocytes from five age-matched individuals with SCZ and five neurotypical controls, upon stimulation with TNF-α (10 ng/mL), affected microglial biology. Transcriptomics, bioinformatics and functional assays were used as readouts.

Results: TNF-□ stimulation of SCZ astrocytes, relative to their control counterparts, triggered increased mRNA expression of pro-inflammatory cytokines and CX3CL1, a chemokine involved in chemotaxis and synapse pruning. Interestingly, transcriptomic and gene set enrichment analyses revealed that reactive SCZ astrocytes promoted the downregulation of biological processes associated with immune cell proliferation and activation, phagocytosis and cell migration in induced microglial-like cells (iMGs). Under such conditions, iMGs assumed a dystrophic/senescent-like phenotype associated with accelerated transcriptional age. Functional validations showed that TNF-□-stimulated SCZ astrocytes promoted reduced synaptoneurosomes phagocytosis by iMGs. Additionally, stimulated astrocytes (control and SCZ) induced iMGs migration in a CX3CR1-dependent manner. Nevertheless, reactive SCZ astrocytes did not promote greater microglial chemotaxis, despite secreting twice as much CX3CL1 compared to stimulated control astrocytes, possibly by lowering CX3CR1 in the plasma membrane.

Conclusions: Altogether, these findings suggest that astrocytes contribute to SCZ pathology by altering normal microglial function and inducing a dystrophic phenotype.

INTRODUCTION

Schizophrenia (SCZ) is a neurodevelopmental disorder with an estimated lifetime prevalence ranging between 0.3-0.7% worldwide (1). Symptoms usually appear between late adolescence and early adulthood (2) and can be divided into three broad categories: positive symptoms, such as hallucinations, psychosis and delusions; negative symptoms, e.g., depressive behavior, distraught thoughts and social withdrawn; and cognitive deficits, including working memory impairments, learning disabilities and attention deficits (3-5).

The causes of SCZ remain poorly understood, as both genetic and environmental risk factors interact to generate susceptible conditions towards the onset of this multifactorial disorder later in life (6-9). Environmental risk factors, including childhood stress, obstetric complications and maternal infection during pregnancy (7, 9), trigger inflammatory signaling cascades, which affect the developing brain at prenatal and early postnatal stages (6, 8). Indeed, genetic, transcriptional and serological evidence indicate increased inflammatory conditions in patients with SCZ, given the enhanced levels of multiple cytokines, such as IL-1β, IL-6, IL-8 and TNF-α (8, 10, 11). Moreover, genetic variants associated with SCZ show dynamic regulatory activity in neural cells in response to cytokine exposure (12).

Astrocytes provide metabolic support to neurons, facilitating the formation and modulation of synaptic connectivity, ionic buffering, while also uptaking and releasing neurotransmitters (13). Along with microglia, astrocytes perceive pro-inflammatory stimulation through a wide range of immune receptors, ultimately leading to their activation (14). Astrocyte activation follows enhanced expression of reactivity markers, such as GFAP and Vimentin, as well as augmented secretion of a wide range of cytokines and chemokines (e.g., TNF-α, IL-6, GM-CSF, TGF-β, CCL2) (13-15). Secretion of these immune factors can, in turn, act upon microglial cells, either boosting or suppressing their activation, greatly impacting their effector capabilities, such as phagocytosis and cell migration (13-15). Astrocytes also modulate microglial function under physiological conditions; for instance, astrocyte-produced IL-33 stimulates synaptic pruning by microglia, which is critical for proper neuronal connectivity (16).

Human genetic, post-mortem, and brain imaging analyses, together with mouse behavioral studies, link astrocytic dysfunction to SCZ (17, 18). Astrocyte and interferon-response gene expression modules were upregulated in patients with SCZ, while the microglia module was downregulated (19). Likewise, PET-scans reveal increased astrocyte reactivity in individuals with SCZ in the anterior cingulate cortex and left hippocampus (20). Finally, human induced pluripotent stem cells (hiPSCs)-derived astrocytes from individuals with SCZ have shown impaired astrocytic differentiation and maturation (21), abnormal calcium signaling (22), decreased glutamate uptake (22), and enhanced pro-inflammatory profile (23, 24).

Nonetheless, the crosstalk between astrocytes and microglia in SCZ, especially under pro-inflammatory conditions, remains unclear. Here we evaluated how reactive SCZ hiPSC-derived astrocytes affected the microglial phenotype, both at the transcriptional and functional levels. We further assessed the contribution of CX3CL1/CX3CR1 axis in this phenomenon and aimed at identifying putative transcriptional factors driving the observed alterations.

MATERIALS AND METHODS

All experiments carried out throughout this work were approved by UFMG's Ethics Committee (COEP-UFMG #90424518.3.1001.5149) and were performed according to the Helsinki Declaration and the Brazilian National Health Council Resolution 466/12.

A detailed description of the following assays can be found in the **Supplementary Information**: astrocytes and neuronal differentiation from hiPSCs, induced microglial-like cells (iMGs) differentiation, RT-qPCR, RNA-sequencing, bioinformatic analyses, Western Blot, ELISA, Cell-based ELISA, immunofluorescence staining, synaptoneurosomes isolation and phagocytosis, cell migration, *Mycoplasma* testing and statistical analyses.

RESULTS

SCZ-sourced astrocytes display increased pro-inflammatory response following stimulation with TNF-α

Given the potential role for astrocytes in SCZ, we screened two transcriptomic (Szabo *et al* (22); Akkouh *et al* (25)) and one proteomic (Trindade *et al* (23)) studies that compared gene/protein expression changes between hiPSC-derived astrocytes from individuals with SCZ and neurotypical controls (HCT), in order to identify common biological processes associated with all three datasets. Interestingly, only the "cellular homeostasis" (GO:0019725) term overlapped among all three (**Figure S1A-B; Tables S1A-C**). Although no single candidate gene from the "cellular homeostasis" term overlapped among all three studies, three genes were present in at least two: CX3CL1 (the sole member of the CX3C chemokine family, also known as Fractalkine), NGFR (Nerve Growth Factor Receptor) and SLC24A2 (a calcium, potassium:sodium antiporter) (**Figures S1C-D**). CX3CL1 is associated with a wide range of biological processes that might be important in the context of SCZ, including microglial migration, immune response and synaptic pruning (**Figure S1E**), the latter having long been hypothesized as having a causative role in this disorder (26, 27). Along with CX3CL1 (28), classical complement components have also been implicated in synaptic elimination (29, 30) (**Figure 1A**), while astrocyte-produced IL-33 has been shown to promote microglial-mediated synaptic uptake (16). In addition, reactive astrocytes display increased expression of a wide range of cytokines with pleiotropic activities (13-15, 31, 32), making them important targets for further investigation.

Taking in consideration the predicted involvement of inflammatory signaling in schizophrenia (8) and TNF-α ability in inducing astrocyte's reactivity (31), we decided to assay the expression of CX3CL1, IL-33, complement components and pro- and anti-inflammatory cytokines in hiPSC-derived astrocytes from five neurotypical (HCT) and five SCZ cases, upon stimulation with TNF-α (**Figure 1B**). Independent of cell donor diagnostic, CX3CL1 and C3 mRNAs were upregulated in astrocytes subjected to TNF-α stimulation, while C1q (subunit C) expression was not detected, and no change was observed in IL-33 and C4 expression (**Figure 1C-F**). Interestingly, CX3CL1 transcripts were higher in stimulated SCZ astrocytes compared to stimulated controls (**Figure**

1E). Moreover, TNF-α stimulation promoted the mRNA upregulation of the pro-inflammatory cytokines CCL5, TNF-α, IL-1α, IL-1β, IL-6 and IL-8, while the anti-inflammatory cytokines IL-4 and IL-10 were not detected (**Figure 1G-L**). Noteworthy, stimulated SCZ astrocytes displayed significantly augmented CCL5, IL-1α, IL-1β and IL-6 (and a trend towards increased TNF-α) mRNA levels compared to stimulated HCT astrocytes (**Figure 1G-K**).

Among these immune factors**,** CX3CL1 has been shown to be involved in a multitude of biological processes relevant in the context of SCZ **(Figure S1E)**. Thus, we sought to validate CX3CL1 mRNA expression findings **(Figure 1E)** at the protein level. TNF-α stimulation increased the production and secretion of CX3CL1 in both HCT and SCZ astrocytes, while no change in expression was observed at the non-secreted protein level **(Figure 1M-O)**. Remarkably, stimulated SCZ astrocytes showed an approximate two-fold augmentation in secreted CX3CL1 levels compared to stimulated control astrocytes **(Figure 1O).** Taken together, these data indicate that SCZ astrocytes responded stronger to TNF-α stimulation by producing greater levels of several pro-inflammatory cytokines and the chemokine CX3CL1, relative to HCT astrocytes.

TNF-α-stimulated SCZ astrocytes promote a dysfunctional transcriptional response in microglial-like cells

Since many pro-inflammatory cytokines and CX3CL1 display pleiotropic functions, being capable of inducing several distinct responses in immune cells (32, 33) (**Figure S1E**), we queried potential biological processes that might be altered in microglial-like cells by reactive SCZ astrocytes. We generated iMGs from a neurotypical individual (**Figure S2**), incubated these cells with astrocyte conditioned media (A_{CM}) harvested from HCT and SCZ astrocytes subjected to either vehicle or TNF-α stimulation (**Figure 1B**), and applied bulk RNA-seq to evaluate the transcriptional profile of these iMGs.

Principal component (PC) analysis showed that iMG samples exposed to A_{CM} SCZ (+TNF-α) clustered separately from iMGs cultured with any other A_{CM} in PC1; otherwise, PC2 segregated iMGs incubated with A_{CM} HCT (+TNF-α) from all other samples. Only the third principal component effectively split

samples based on A_{CM} sourced from either HCT or SCZ astrocytes **(Figure 2A)**. Larger transcriptional differences were observed when iMGs were exposed to A_{CM} from TNF-α-stimulated astrocytes. Indeed, 414 differentially expressed genes (DEGs) (326 up- and 88 downregulated) were identified in iMGs + A_{CM} HCT (+TNF-α), while 847 DEGs (388 up- and 459 downregulated) were found in iMGs + A_{CM} SCZ (+TNF-α), and only 110 DEGs (83 up- and 27 downregulated) were detected in iMGs + A_{CM} SCZ (N.S.) **(Figure 2B-C; Tables S2A-C)**. Surprisingly, the iMGs + A_{CM} SCZ (N.S.) group shared more DEGs in common with iMGs + A_{CM} HCT (+TNF-α) (51 DEGs) than with iMGs + A_{CM} SCZ (+TNF-α) (14 DEGs) **(Figure 2B)**. These data corroborate the PC analysis results, since the first two groups are clustered closer in PC1 compared to the latter **(Figure 2A).**

Gene set enrichment analysis (GSEA) further explored the biological processes (GO terms) associated with each experimental condition. Incubation with A_{CM} SCZ (+TNF-α) led to the substantial downregulation of GO terms associated with several important microglial functions, including immune cell activation and proliferation, response to hypoxia, chemotaxis, cell migration and phagocytosis. A limited amount of downregulated GO terms was also shared with iMGs + A_{CM} HCT (+TNF-α), such as receptor-mediated endocytosis, regulation of autophagy, endosomal and lysosomal transport **(Figure 2D; Table S3A).** A closer inspection of the DEGs related to these downregulated GO terms unraveled that this molecular phenotype in iMGs + A_{CM} SCZ (+TNF-α) was mainly driven by decreased expression of cytokines and chemokines (e.g., *CCL2, CCL13, CCL18*), and immune and phagocytic receptors (e.g., *FPR1, TREM1, TREM2, MERTK, MARCO, IL2RA, IL2RB*) **(Figure 2E; Tables S2A-C and S3A).** Conversely, both TNF-α-stimulated HCT and SCZ astrocytes induced the upregulation GO terms associated with ribosome biogenesis, response to virus and cellular response to interferon (IFN) in iMGs**.** However, while stimulated HCT astrocytes promoted an increase in both type I and type II IFN response, stimulated SCZ astrocytes only promoted the upregulation of response to IFN-β, a type I IFN, suggesting a restricted response by iMGs to IFN when exposed to A_{CM} from the latter compared to the former**.** Furthermore, TNF-α stimulation begot a shift in the direction of iMGs' biological processes

prompted by SCZ astrocytes. For example, while iMGs + A_{CM} SCZ (N.S.) displayed the upregulation of GO terms associated with chemotaxis, immune cell activation and proliferation, as well as the downregulation of processes related to mitochondrial metabolism, the contrary pattern was observed in iMGs + A_{CM} SCZ (+ TNF-α) **(Figure 2D, Table S3A)**.

To confirm these results, we carried out GSEA using KEGG pathways. Indeed, we confirmed that both A_{CM} HCT (+TNF-α) and A_{CM} SCZ (+TNF-α) induced the downregulation of lysosomal and autophagy pathways, while only the latter promoted a significant reduction in the endocytic pathway **(Figure S3; Table S3B)**. Noteworthy, TNF-α-stimulated SCZ astrocytes also triggered the upregulation of the p53 signaling pathway, reactive oxygen species production and multiple neurodegenerative disorders (e.g. Alzheimer's and Parkinson's Diseases) in iMGs, in marked contrast to iMGs + A_{CM} SCZ (N.S) **(Figure S3; Table S3B).**

To gain a better insight into how reactive SCZ astrocytes induce the downregulation of biological processes and pathways implicated in important microglial functions, we undertook a systems biology approach to establish whether their genes are organized into recognizable co-expression modules. Weighted gene co-expression network analysis resolved 35 modules **(Figure 3A; Figure S4A-B, Table S4).** GO term overrepresentation analysis identified the biological processes associated with each module. The *brown* and *blueviolet* modules were largely enriched for terms involved in regulation of immune cell activation, autophagy, cell division and migration, chemotaxis, phagocytosis and endocytosis **(Figure 3B-C; Table S5).** Notably, these two modules were negatively correlated with iMGs incubated with A_{CM} SCZ (+TNF-α) and positively correlated with iMGs + A_{CM} SCZ (N.S.) **(Figure 3A).** Furthermore, the *antiquewhite2* and *lightgreen* modules, positively correlated with iMGs + A_{CM} SCZ (+TNF-α) samples, were enriched for GO terms linked to mitochondrial metabolism **(Figures 3A and S4C-D; Table S5).** On the other hand, the *darkolivegreen2* and *palevioletred* modules were positively correlated with iMGs cultured in the presence of A_{CM} HCT (+TNF-α) **(Figure 3A).** These two modules were mainly associated with biological processes related to response to cytokine and chemokine stimulation, as well as regulation of

response to viruses and IFN **(Figure 3D; Figure S4E; Table S5).** Altogether, these findings corroborate the GSEA results **(Figure 2D)** and suggest that SCZ genetic background and pro-inflammatory stimulation, such as by TNF-α, are simultaneously required in astrocytes to make microglial-like cells assume a dysfunctional molecular phenotype.

Master Regulator Analysis (MRA) reveals transcription factors involved in establishing the microglial dysfunctional response

Since co-expressed genes often share common regulators, including upstream transcription factors (TFs), we performed *in silico* master regulator analysis (MRA) using a comprehensive list of human TFs (34) to identify prospective regulators in our dataset. A total of 161 regulons were identified, of which 126 were shared between at least two groups, 5 were exclusive to iMGs + A_{CM} HCT (+TNF-α) and 30 only found in iMGs + A_{CM} SCZ (+TNF-α) **(Figure S5A; Tables S6A-C).** Next, we calculated the predicted activity status of these transcription factors and only kept those whose activity were either considered as activated or repressed in at least one experimental group **(Figures S5B-D and S6; Tables S6A-C)**. To assess putative TFs regulating the co-expressed gene networks, we carefully cross-examined the target genes regulated by each TF and the gene sets pertaining to each WGCNA module. IRF1, whose activity status was predicted to be activated and was the only TF exclusive to iMGs + A_{CM} HCT (+TNF-α) **(Figures S5B and S6, Table S6A)**, was associated with the *darkolivegreen2* module **(Figure 3E)**, pointing to its possible role in inducing the expression of genes involved in response to cytokine, such as IFN, and chemokine stimulation in this experimental group. Interestingly, we found four (HHEX, SOX4, MEF2C and NFATC2) and two (CENPA and MXD3) TFs connected to the *brown* and *blueviolet* modules, respectively. MEF2C was also the only TF associated with the *antiquewhite2* module **(Figure 3E).** Except for SOX4, all these putative TFs had predicted repressed activity in the iMGs + A_{CM} SCZ (+TNF-α) group **(Figures S5D and S6, Table S6C)**. Among them, we observed that *MEF2C* mRNA expression was significantly reduced in iMGs cultured in the presence of A_{CM} SCZ (+TNF-α), while *NFATC2* and *CENPA* trended in the same direction **(Figure 2C and Table S2C)**. These data point to

a putative role of MEF2C, NFATC2 and CENPA in promoting the dysfunctional microglial phenotype triggered by reactive SCZ astrocytes.

Reactive SCZ astrocytes induce iMGs to assume a dystrophic/senescent-like phenotype

We were also puzzled by our results indicating that TNF-α-stimulated SCZ astrocytes promoted the upregulation of pathways associated with multiple neurodegenerative diseases, such as Alzheimer's (AD) and Parkinson's disease **(Figure S3 and Table S3B)**, and decided to investigate whether reactive SCZ astrocytes could prompt these dysfunctional microglia to assume a molecular profile akin to those observed in such neurological disorders. Hence, our dataset was compared to microglial transcriptional signatures from human prefrontal cortex (PFC) brain samples obtained from patients with AD (35). iMGs cultured with A_{CM} SCZ (N.S.) showed a positive association with the "interferon ELN (endolysosomal network)" signature, while iMG + A_{CM} HCT (+TNF-α) was associated with the "canonical inflammatory" and "cell cycle" ones**.** Remarkably, iMGs incubated with A_{CM} SCZ (+TNF-α) were found to be positively enriched for the "dystrophic" microglial phenotype **(Figure 4A)**.

Dystrophic microglia display morphological, molecular and functional alterations characteristic of aged and senescent microglia (36-40). Then, we evaluated whether A_{CM} SCZ (+TNF-α) induced a senescent-like state in iMGs by assessing their transcriptional profile against the CellAge database (41). Interestingly, iMG + A_{CM} SCZ (+TNF-α) displayed a positive association with genes that either induce or have a context-dependent regulatory activity ("unclear" category) towards cellular senescence, whilst iMG + A_{CM} HCT (+TNF-α) was also positively enriched for genes that display an inhibitory role **(Figure 4B).** To confirm these results, we analyzed the expression of some senescence markers (42) in our RNA-seq dataset. Curiously, reactive SCZ astrocytes induced the mRNA expression of more senescent markers (*IL-1α, CDKN1A, CDKN2B, SERPINE1* and *MMP12*) in iMGs than their reactive HCT counterparts (*IL-1α, SERPINE1* and *MMP12*), with the former displaying an even greater expression of *MMP12* than the latter **(Figure 4C-G)**. In addition,

iMG + A_{CM} HCT (+TNF-α) showed the augmented expression of *MKI67,* a well-known proliferation marker, while the contrary was observed in iMG + A_{CM} SCZ (+TNF-α) **(Figure 4H)**, indicating a potential downregulation in cell proliferation, a cellular senescence hallmark (42).

Finally, iMGs' transcriptional age was calculated to verify whether reactive SCZ astrocytes promoted accelerated aging, thus potentially leading to this dystrophic microglial phenotype. Intriguingly, exposure to both A_{CM} HCT (+TNF-α) and A_{CM} SCZ (+TNF-α) significantly increased the transcriptional age of iMGs, while no difference was observed between A_{CM} SCZ (N.S.) and A_{CM} HCT (N.S.) (+0.275 vs 0.000 years-old). Nonetheless, this transcriptional age enhancement was almost two-fold greater in iMGs incubated with A_{CM} SCZ (+TNF-α) than A_{CM} HCT (+TNF-α) (+7.593 vs. +3.831 years-old) **(Figure 4I).** Taken together, these results suggest that reactive SCZ astrocytes trigger accelerated aging in iMGs, prompting them to assume a dystrophic/senescent-like phenotype.

Reactive SCZ astrocytes impair iMGs' synaptic engulfment

Phagocytosis is among the key functions impaired in dystrophic microglia (36), whose GO term was downregulated in iMGs after exposure to A_{CM} SCZ (+TNF-α) **(Figure 2D).** Given the strong association between synaptic uptake by microglial cells and SCZ development, we decided to assess whether reactive SCZ astrocytes could affect microglial engulfment of synaptic material **(Figure 5A)**. To establish this assay, we first isolated synaptoneurosomes from mature hiPSC-derived neurons **(Figure S7A-E),** fluorescently-labeled them and added to iMG cultures. As can be seen in **Figure S7F** and **Movie S1**, iMGs were able to successfully phagocytose labeled synaptoneurosomes. Next, we tested whether A_{CM} from reactive SCZ astrocytes affected iMGs' phagocytosis **(Figure 5A)**. Interestingly, incubation with A_{CM} SCZ (+TNF-α) was the only condition capable of diminishing synaptic engulfment by iMGs **(Figure 5B-E, Figure S8 and S9A).**

Considering this result, we revisited our initial screening to select a potential target that could modulate this process **(Figure 1)**. We chose CX3CL1,

as it has been previously shown to mediate synapse elimination (28), and also displayed augmented secretion by stimulated SCZ astrocytes relative to stimulated controls **(Figure 1O)**. Then, to further evaluate its role, iMGs were incubated in the presence recombinant CX3CL1 (rCX3CL1), at approximately the same concentration secreted by reactive SCZ astrocytes **(Figure S9B).** Intriguingly, rCX3CL1 diminished synaptoneurosomes uptake by iMGs **(Figure S9C-D).** Next, we tested whether A_{CM} ACZ (+ TNF-α) required CX3CL1 signaling to lessen iMGs' phagocytosis **(Figure 5A)**. Indeed, the pharmacological blockade of CX3CR1 by AZD8797 increased synaptoneurosomes engulfment relative to vehicle-treated iMGs under control conditions (A_{CM} HCT (N.S.)) **(Figure 5B-E, Figure S8, Figure S9E).** Nevertheless, CX3CR1 inhibition did not rescue the reduction in synaptoneurosomes phagocytosis by iMGs when incubated with A_{CM} SCZ (+TNF-α), nor did it lead to enhanced synaptic material uptake in iMGs cultured with either A_{CM} HCT (+TNF-α) or A_{CM} SCZ (N.S.), indicating that CX3CL1 was not responsible for promoting the observed phenotype **(Figure 5B-E)**. Overall, these data suggest that reactive SCZ astrocytes hinder microglial synaptic material phagocytosis. However, these effects on iMGs were CX3CL1-independent, not being reversed by the pharmacological inhibition of its receptor.

TNF-α-stimulated SCZ astrocytes limit microglial migration

Cell migration is another phenomenon impaired in senescent microglia (36), whose CX3CL1 involvement has already been demonstrated **(Figure S1E)**. Hence, we next queried whether reactive SCZ astrocytes affected microglial chemotaxis**.** iMGs exposure to A_{CM} from either TNF-α-stimulated HCT or SCZ astrocytes significantly enhanced microglial migration in a CX3CR1-dependent manner **(Figures 6A-B)**. Nonetheless, although reactive SCZ astrocytes secreted almost twice as much CX3CL1 relative to their stimulated control counterparts, there was no difference in their capacity to induce microglial chemotaxis **(Figures 6A-B).**

Intriguingly, age-dependent decreases in CX3CR1 surface levels have been observed in human circulating monocytes (43). To assess whether this phenomenon could potentially limit iMGs' response to reactive SCZ astrocytes-secreted CX3CL1, we measured the total and plasma membrane levels of CX3CR1 in iMGs exposed to A_{CM} for 24 h. SCZ A_{CM} (but not A_{CM} HCT (+ TNF-α)) diminished CX3CR1 plasma membrane content in iMGs, while total CX3CR1 levels remained unchanged **(Figure 6C-D)**. Taken together, these results indicate that both transcriptional repression of chemotaxis-related biological processes and diminution of CX3CR1 plasma membrane levels prompted by reactive SCZ astrocytes act in concert to restrict microglial-like cells migratory capabilities.

DISCUSSION

Multiple lines of evidence link microglia and astrocytes to neuropathological mechanisms in SCZ (19-23, 44, 45), yet little is known about how these glial cells communicate and regulate each other's function in this disorder. Here, we applied a combination of functional assays and transcriptomics to determine how SCZ astrocytes modulate key aspects of microglial biology. Reactive SCZ astrocytes displayed a stronger response to pro-inflammatory stimulation, that, in turn, prompted microglial-like cells to assume a dystrophic/senescent-like phenotype. Indeed, we observed that these dysfunctional microglia display features often found in aged microglia, including the upregulation of senescence markers (e.g., *CDKN1A, CDKN2B* and *MMP12*) and pathways (p53 signaling pathway), and the downregulation of several biological processes linked to cell proliferation, phagocytosis and chemotaxis. Our functional assays confirmed the occurrence of these last two phenomena by showing impairments in synaptic phagocytosis and limited microglial migration in a CX3CL1-independent and CX3CL1-dependent fashion, respectively. Supporting this hypothesis, *post-mortem* findings reported augmented lipofuscin granules in microglia from younger and older individuals with SCZ, another characteristic cellular senescence feature (45, 46). Furthermore, plenty of studies using anatomical, imaging, proteomic, metabolomic and epigenomic techniques have suggested that individuals with

SCZ display accelerated brain aging (47-54). In addition, aged and senescent microglia, as well as other myeloid cells, have been shown to display impaired phagocytosis and cell migration (36, 55-59).

A potential link between senescent immune cells and the CX3CL1/CX3CRI axis was provided by Seidler *et al* (43). Indeed, the authors found that circulating monocytes harvested from older donors show diminished CX3CR1 surface expression, alike what we observed in iMGs exposed to SCZ A_{CM} (43). Given that CX3CR1 mRNA is downregulated in the blood and brain of patients with SCZ (19, 60, 61), and knowing that the $CX3CR1^{A55T}$ loss of function variant was identified as a SCZ risk factor (62), we suggest that activated astrocytes contribute to the CX3CL1/CX3CR1 axis dysfunction in SCZ. Yet, one seeming contradiction in our results is that reactive SCZ astrocytes secreted twice the amount of CX3CL1 compared to HCT counterparts, but did not induce a stronger migratory response in iMGs. One possible explanation lies in the reduction in the CX3CR1 cell surface content in iMGs when incubated with ACM SCZ (+TNF-α), along with the possible existence of alternate pathways leading to the transcriptional dysregulation of cell migration, as indicated by our results. Altogether, these results suggest that activated astrocytes disturb microglial CX3CL1/CX3CR1 signaling in SCZ.

We also employed computational methods to find putative transcription factors capable of promoting the microglial phenotypic transition observed here. We identified three potential candidates (MEF2C, NFATC2 and CENPA), whose predicted repressed activities in iMGs incubated with A_{CM} SCZ (+TNF-α) may be responsible for downregulating the expression of genes associated with immune cell activation and proliferation, chemotaxis and phagocytosis. Intriguingly, MEF2C and NFATC2 have already been implicated in SCZ (63-65), while decreased expression of MEFC2 and CENPA are associated with increased aging in microglia and p53-dependent senescence induction in fibroblasts, respectively (66, 67). These data suggest a potential mechanism explaining, at least in part, how reactive SCZ astrocytes prompt iMGs to assume a senescent-like state. However, a thorough validation about how each TF affects microglia in the context of SCZ is beyond the scope of this work.

In summary, our results demonstrated that reactive SCZ astrocytes led to substantial alterations in microglial biology, both at functional and transcriptional levels. These findings should be viewed as part of a grander change in the immune response landscape of microglia. Taken together, they strengthen the hypothesis that SCZ development requires the simultaneous presence of a susceptible genetic background and external environmental stimuli (8).

ACKNOWLEDGEMENTS

We acknowledge the contributions on technical support of Mr. Jamil Silvano de Oliveira, Mr. Samuel Tadeu Rocha, Mr. Leandro Costa Nascimento, Dr. João Trindade Marques, all current and former members of the Laboratory of Neurobiochemistry (UFMG, Belo Horizonte, Brazil) and all medical and nursery personnel at the Borges da Costa Clinic (UFMG Clinic's Hospital, Belo Horizonte, Brazil). We also thank Dr. João Paulo Pereira de Almeida, Dr. Álvaro Gil Araújo Ferreiro and Ms. Sophie Turetsky Cohen for their valuable discussions and insights regarding this work. This research project was funded by Conselho Nacional de Desenvolvimento Científico e Tecnológico (CNPq) grants 441719/2020-1 and 403171/2023-7 and Fundação de Amparo à Pesquisa do Estado de Minas Gerais (FAPEMIG) grants APQ-03921-22 and APQ-00140-23. P.L.C. was recipient of CNPq and Fulbright scholarships during this work and is currently recipient of CAPES/Print fellowship; J.P.S.L. and N.C.S. are recipients of CNPq graduate scholarships.

P.L.C. and F.M.R. conceived and designed the study. P.L.C. performed candidate genes screening, total RNA extraction, hiPSCs-derived neurons characterization, synaptoneurosomal characterization, iMGs synaptoneurosomes engulfment analysis pipeline development and quantification, western blots, ELISA, cell-based ELISA and iMGs migration assay. G.V. differentiated hiPSCs to NSCs. G.V. and J.C.P.M. characterized hiPSCs and NSCs. P.L.C., J.P.S.L. and P.T. differentiated hiPSC-derived astrocytes. P.T. characterized hiPSC-derived astrocytes. P.L.C. and J.P.S.L. performed astrocytes stimulation, RT-qPCR experiments, hiPSC-derived neuronal differentiation, iMGs differentiation and characterization. P.L.C. and

J.S.F. performed synaptoneurosomes isolation and synaptoneurosomal phagocytosis assay. J.P.S.L. carried out iMGs migration assay blind quantification. B.F.C. performed PBMC's donor psychiatric evaluation. R.N. supervised PBMC's donor candidate recruitment and helped to draft ethics committee protocol. N.C.S. drew whole blood from neurotypical donor. P.L.C., N.C.S. and R.C.C. performed PBMCs isolation from whole blood. R.C.C. and J.S.F. helped to standardize ELISA and cell-based ELISA protocols. P.L.C., P.T. and L.C. established iMGs differentiation protocol. M.H.B. supervised iMGs differentiation protocol establishment. Y.M.H.T. performed RNA quality assessment in Bioanalyzer. P.L.C. and I.J.S.F. prepared cDNA libraries prior to RNA-sequencing. P.L.C. and C.Y.L. conducted bioinformatic analyses and carried out statistical analyses. K.J.B. provided platforms for bioinformatic analysis. K.J.B. and F.M.R. supervised bioinformatic analysis. S.K.R. supervised hiPSC-derived NSCs and astrocytes differentiations and donated NSCs and astrocytes cell lines, generated in his laboratory. P.L.C. and F.M.R. prepared the manuscript. L.B.V. provided research funding. F.M.R. supervised this study and obtained research grant funding. All researchers involved in this study read, made their contribution to the final version of this manuscript and agreed to publish this work.

DISCLOSURES

Authors declare no conflict of interest.

REFERENCES

1. Solmi M, Seitidis G, Mavridis D, Correll CU, Dragioti E, Guimond S, et al. (2023): Incidence, prevalence, and global burden of schizophrenia - data, with critical appraisal, from the Global Burden of Disease (GBD) 2019. *Mol Psychiatry*. 28:5319-5327.

2. Hafner H, Maurer K, Loffler W, Riecher-Rossler A (1993): The influence of age and sex on the onset and early course of schizophrenia. *Br J Psychiatry*. 162:80-86.

3. Cannon TD (2015): How Schizophrenia Develops: Cognitive and Brain Mechanisms Underlying Onset of Psychosis. *Trends Cogn Sci*. 19:744-756.

4. Perez SM, Lodge DJ (2014): New approaches to the management of schizophrenia: focus on aberrant hippocampal drive of dopamine pathways. *Drug Des Devel Ther*. 8:887-896.

5. Sakurai T, Gamo NJ, Hikida T, Kim SH, Murai T, Tomoda T, et al. (2015): Converging models of schizophrenia--Network alterations of prefrontal cortex underlying cognitive impairments. *Prog Neurobiol*. 134:178-201.

6. Hilker R, Helenius D, Fagerlund B, Skytthe A, Christensen K, Werge TM, et al. (2018): Heritability of Schizophrenia and Schizophrenia Spectrum Based on the Nationwide Danish Twin Register. *Biol Psychiatry*. 83:492-498.

7. Lipner E, Murphy SK, Ellman LM (2019): Prenatal Maternal Stress and the Cascade of Risk to Schizophrenia Spectrum Disorders in Offspring. *Curr Psychiatry Rep*. 21:99.

8. Muller N, Weidinger E, Leitner B, Schwarz MJ (2015): The role of inflammation in schizophrenia. *Front Neurosci*. 9:372.

9. Nimgaonkar VL, Prasad KM, Chowdari KV, Severance EG, Yolken RH (2017): The complement system: a gateway to gene-environment interactions in schizophrenia pathogenesis. *Mol Psychiatry*. 22:1554-1561.

10. Frydecka D, Krzystek-Korpacka M, Lubeiro A, Stramecki F, Stanczykiewicz B, Beszlej JA, et al. (2018): Profiling inflammatory signatures of schizophrenia: A cross-sectional and meta-analysis study. *Brain Behav Immun*. 71:28-36.

11. Rodrigues-Amorim D, Rivera-Baltanas T, Spuch C, Caruncho HJ, Gonzalez-Fernandez A, Olivares JM, et al. (2018): Cytokines dysregulation in schizophrenia: A systematic review of psychoneuroimmune relationship. *Schizophr Res*. 197:19-33.

12. Retallick-Townsley KG, Lee S, Cartwright S, Cohen S, Sen A, Jia M, et al. (2024): Dynamic stress- and inflammatory-based regulation of psychiatric risk loci in human neurons. *bioRxiv*.

13. Bernaus A, Blanco S, Sevilla A (2020): Glia Crosstalk in Neuroinflammatory Diseases. *Front Cell Neurosci*. 14:209.

14. Linnerbauer M, Wheeler MA, Quintana FJ (2020): Astrocyte Crosstalk in CNS Inflammation. *Neuron*. 108:608-622.

15. Liu W, Tang Y, Feng J (2011): Cross talk between activation of microglia and astrocytes in pathological conditions in the central nervous system. *Life Sci*. 89:141-146.

16. Vainchtein ID, Chin G, Cho FS, Kelley KW, Miller JG, Chien EC, et al. (2018): Astrocyte-derived interleukin-33 promotes microglial synapse engulfment and neural circuit development. *Science*. 359:1269-1273.

17. de Oliveira Figueiredo EC, Cali C, Petrelli F, Bezzi P (2022): Emerging evidence for astrocyte dysfunction in schizophrenia. *Glia*. 70:1585-1604.

18. Dietz AG, Goldman SA, Nedergaard M (2020): Glial cells in schizophrenia: a unified hypothesis. *Lancet Psychiatry*. 7:272-281.

19. Gandal MJ, Zhang P, Hadjimichael E, Walker RL, Chen C, Liu S, et al. (2018): Transcriptome-wide isoform-level dysregulation in ASD, schizophrenia, and bipolar disorder. *Science*. 362.

20. Kim M, Choi W, Choi S, Oh H, Kim J, Lee J, et al. (2024): In Vivo Reactive Astrocyte Imaging in Patients With Schizophrenia Using Fluorine 18-Labeled THK5351. *JAMA Netw Open*. 7:e2410684.

21. Windrem MS, Osipovitch M, Liu Z, Bates J, Chandler-Militello D, Zou L, et al. (2017): Human iPSC Glial Mouse Chimeras Reveal Glial Contributions to Schizophrenia. *Cell Stem Cell*. 21:195-208 e196.

22. Szabo A, Akkouh IA, Vandenberghe M, Osete JR, Hughes T, Heine V, et al. (2021): A human iPSC-astroglia neurodevelopmental model reveals divergent transcriptomic patterns in schizophrenia. *Transl Psychiatry*. 11:554.

23. Trindade P, Nascimento JM, Casas BS, Monteverde T, Gasparotto J, Ribeiro CT, et al. (2023): Induced pluripotent stem cell-derived astrocytes from patients with schizophrenia exhibit an inflammatory phenotype that affects vascularization. *Mol Psychiatry*. 28:871-882.

24. Koskuvi M, Lehtonen S, Trontti K, Keuters M, Wu YC, Koivisto H, et al. (2022): Contribution of astrocytes to familial risk and clinical manifestation of schizophrenia. *Glia*. 70:650-660.

25. Akkouh IA, Hribkova H, Grabiec M, Budinska E, Szabo A, Kasparek T, et al. (2022): Derivation and Molecular Characterization of a Morphological Subpopulation of Human iPSC Astrocytes Reveal a Potential Role in Schizophrenia and Clozapine Response. *Schizophr Bull*. 48:190-198.

26. Feinberg I (1982): Schizophrenia: caused by a fault in programmed synaptic elimination during adolescence? *J Psychiatr Res*. 17:319-334.

27. Howes OD, Onwordi EC (2023): The synaptic hypothesis of schizophrenia version III: a master mechanism. *Mol Psychiatry*. 28:1843-1856.

28. Paolicelli RC, Bolasco G, Pagani F, Maggi L, Scianni M, Panzanelli P, et al. (2011): Synaptic pruning by microglia is necessary for normal brain development. *Science*. 333:1456-1458.

29. Stevens B, Allen NJ, Vazquez LE, Howell GR, Christopherson KS, Nouri N, et al. (2007): The classical complement cascade mediates CNS synapse elimination. *Cell*. 131:1164-1178.

30. Yilmaz M, Yalcin E, Presumey J, Aw E, Ma M, Whelan CW, et al. (2021): Overexpression of schizophrenia susceptibility factor human complement C4A promotes excessive synaptic loss and behavioral changes in mice. *Nat Neurosci*. 24:214-224.

31. Trindade P, Loiola EC, Gasparotto J, Ribeiro CT, Cardozo PL, Devalle S, et al. (2020): Short and long TNF-alpha exposure recapitulates canonical astrogliosis events in human-induced pluripotent stem cells-derived astrocytes. *Glia*. 68:1396-1409.

32. Moraga I, Spangler J, Mendoza JL, Garcia KC (2014): Multifarious determinants of cytokine receptor signaling specificity. *Adv Immunol*. 121:1-39.

33. Mecca C, Giambanco I, Donato R, Arcuri C (2018): Microglia and Aging: The Role of the TREM2-DAP12 and CX3CL1-CX3CR1 Axes. *Int J Mol Sci*. 19.

34. Lambert SA, Jolma A, Campitelli LF, Das PK, Yin Y, Albu M, et al. (2018): The Human Transcription Factors. *Cell*. 172:650-665.

35. Prater KE, Green KJ, Mamde S, Sun W, Cochoit A, Smith CL, et al. (2023): Human microglia show unique transcriptional changes in Alzheimer's disease. *Nat Aging*. 3:894-907.

36. Angelova DM, Brown DR (2019): Microglia and the aging brain: are senescent microglia the key to neurodegeneration? *J Neurochem*. 151:676-688.

37. Lopes KO, Sparks DL, Streit WJ (2008): Microglial dystrophy in the aged and Alzheimer's disease brain is associated with ferritin immunoreactivity. *Glia*. 56:1048-1060.

38. Rim C, You MJ, Nahm M, Kwon MS (2024): Emerging role of senescent microglia in brain aging-related neurodegenerative diseases. *Transl Neurodegener*. 13:10.

39. Shahidehpour RK, Higdon RE, Crawford NG, Neltner JH, Ighodaro ET, Patel E, et al. (2021): Dystrophic microglia are associated with neurodegenerative disease and not healthy aging in the human brain. *Neurobiol Aging*. 99:19-27.

40. Streit WJ, Sammons NW, Kuhns AJ, Sparks DL (2004): Dystrophic microglia in the aging human brain. *Glia*. 45:208-212.

41. Avelar RA, Ortega JG, Tacutu R, Tyler EJ, Bennett D, Binetti P, et al. (2020): A multidimensional systems biology analysis of cellular senescence in aging and disease. *Genome Biol*. 21:91.

42. Suryadevara V, Hudgins AD, Rajesh A, Pappalardo A, Karpova A, Dey AK, et al. (2024): SenNet recommendations for detecting senescent cells in different tissues. *Nat Rev Mol Cell Biol*.

43. Seidler S, Zimmermann HW, Bartneck M, Trautwein C, Tacke F (2010): Age-dependent alterations of monocyte subsets and monocyte-related chemokine pathways in healthy adults. *BMC Immunol*. 11:30.

44. Koskuvi M, Porsti E, Hewitt T, Rasanen N, Wu YC, Trontti K, et al. (2024): Genetic contribution to microglial activation in schizophrenia. *Mol Psychiatry*.

45. Uranova NA, Vikhreva OV, Rakhmanova VI (2021): Abnormal microglial reactivity in gray matter of the prefrontal cortex in schizophrenia. *Asian J Psychiatr*. 63:102752.

46. Uranova NA, Vikhreva OV, Rakhmanova VI, Orlovskaya DD (2020): Dystrophy of Oligodendrocytes and Adjacent Microglia in Prefrontal Gray Matter in Schizophrenia. *Front Psychiatry*. 11:204.

47. Kaufmann T, van der Meer D, Doan NT, Schwarz E, Lund MJ, Agartz I, et al. (2019): Common brain disorders are associated with heritable patterns of apparent aging of the brain. *Nat Neurosci*. 22:1617-1623.

48. Lin CW, Chang LC, Ma T, Oh H, French B, Puralewski R, et al. (2021): Older molecular brain age in severe mental illness. *Mol Psychiatry*. 26:3646-3656.

49. Stone WS, Phillips MR, Yang LH, Kegeles LS, Susser ES, Lieberman JA (2022): Neurodegenerative model of schizophrenia: Growing evidence to support a revisit. *Schizophr Res*. 243:154-162.

50. Campeau A, Mills RH, Stevens T, Rossitto LA, Meehan M, Dorrestein P, et al. (2022): Multi-omics of human plasma reveals molecular features of dysregulated inflammation and accelerated aging in schizophrenia. *Mol Psychiatry*. 27:1217-1225.

51. Ling E, Nemesh J, Goldman M, Kamitaki N, Reed N, Handsaker RE, et al. (2024): A concerted neuron-astrocyte program declines in ageing and schizophrenia. *Nature*. 627:604-611.

52. Caspi A, Shireby G, Mill J, Moffitt TE, Sugden K, Hannon E (2024): Accelerated Pace of Aging in Schizophrenia: Five Case-Control Studies. *Biol Psychiatry*. 95:1038-1047.

53. Constantinides C, Han LKM, Alloza C, Antonucci LA, Arango C, Ayesa-Arriola R, et al. (2023): Brain ageing in schizophrenia: evidence from 26 international cohorts via the ENIGMA Schizophrenia consortium. *Mol Psychiatry*. 28:1201-1209.

54. Tian YE, Cropley V, Maier AB, Lautenschlager NT, Breakspear M, Zalesky A (2023): Heterogeneous aging across multiple organ systems and prediction of chronic disease and mortality. *Nat Med*. 29:1221-1231.

55. Caldeira C, Oliveira AF, Cunha C, Vaz AR, Falcao AS, Fernandes A, et al. (2014): Microglia change from a reactive to an age-like phenotype with the time in culture. *Front Cell Neurosci*. 8:152.

56. Spittau B (2017): Aging Microglia-Phenotypes, Functions and Implications for Age-Related Neurodegenerative Diseases. *Front Aging Neurosci*. 9:194.

57. Yanguas-Casas N, Crespo-Castrillo A, Arevalo MA, Garcia-Segura LM (2020): Aging and sex: Impact on microglia phagocytosis. *Aging Cell*. 19:e13182.

58. Sharma R (2021): Perspectives on the dynamic implications of cellular senescence and immunosenescence on macrophage aging biology. *Biogerontology*. 22:571-587.

59. Hearps AC, Martin GE, Angelovich TA, Cheng WJ, Maisa A, Landay AL, et al. (2012): Aging is associated with chronic innate immune activation and dysregulation of monocyte phenotype and function. *Aging Cell*. 11:867-875.

60. Chamera K, Szuster-Gluszczak M, Basta-Kaim A (2021): Shedding light on the role of CX3CR1 in the pathogenesis of schizophrenia. *Pharmacol Rep*. 73:1063-1078.

61. Snijders G, van Zuiden W, Sneeboer MAM, Berdenis van Berlekom A, van der Geest AT, Schnieder T, et al. (2021): A loss of mature microglial markers without immune activation in schizophrenia. *Glia*. 69:1251-1267.

62. Ishizuka K, Fujita Y, Kawabata T, Kimura H, Iwayama Y, Inada T, et al. (2017): Rare genetic variants in CX3CR1 and their contribution to the increased risk of schizophrenia and autism spectrum disorders. *Transl Psychiatry*. 7:e1184.

63. Cosgrove D, Whitton L, Fahey L, P OB, Donohoe G, Morris DW (2021): Genes influenced by MEF2C contribute to neurodevelopmental disease via gene expression changes that affect multiple types of cortical excitatory neurons. *Hum Mol Genet*. 30:961-970.

64. Mitchell AC, Javidfar B, Pothula V, Ibi D, Shen EY, Peter CJ, et al. (2018): MEF2C transcription factor is associated with the genetic and epigenetic risk architecture of schizophrenia and improves cognition in mice. *Mol Psychiatry*. 23:123-132.

65. Shimamoto-Mitsuyama C, Nakaya A, Esaki K, Balan S, Iwayama Y, Ohnishi T, et al. (2021): Lipid Pathology of the Corpus Callosum in Schizophrenia and the Potential Role of Abnormal Gene Regulatory Networks with Reduced Microglial Marker Expression. *Cereb Cortex*. 31:448-462.

66. Deczkowska A, Matcovitch-Natan O, Tsitsou-Kampeli A, Ben-Hamo S, Dvir-Szternfeld R, Spinrad A, et al. (2017): Mef2C restrains microglial inflammatory response and is lost in brain ageing in an IFN-I-dependent manner. *Nat Commun*. 8:717.

67. Maehara K, Takahashi K, Saitoh S (2010): CENP-A reduction induces a p53-dependent cellular senescence response to protect cells from executing defective mitoses. *Mol Cell Biol*. 30:2090-2104.

FIGURE LEGENDS

FIGURE 1: SCZ astrocytes showed stronger pro-inflammatory response upon TNF-α stimulation. (A) Synaptic pruning proteins network, highlighting CX3CL1 (blue) and classical complement components (yellow): C1q (subunit C), C3 and C4. Macromolecular complexes are drawn as hexagons and individual proteins as round rectangles. **(B)** Experimental design of hiPSC-derived astrocytes differentiation, stimulation with TNF-α (10 ng/mL) and downstream assays (RT-qPCR and conditioned media harvest for further applications). *Schematic picture was drawn using Biorender*. **(C-L)** mRNA expression of C3 **(C)**, C4 **(D),** CX3CL1 **(E),** IL-33 **(F),** CCL5 **(G),** TNF-α **(H),** IL-1α **(I),** IL-1β **(J)**, IL-6 **(K)** and IL-8 **(L)** in HCT and SCZ astrocytes stimulated with TNF-α. *n = 8-10 (two replicates x number of donor cell lines per group).* **(M-O)** Representative Western blot of non-secreted CX3CL1 in HCT and SCZ astrocytes stimulated with 10 ng/mL TNF-α **(M)** and its respective densitometric quantification **(N)**. *Representative blot out of three independent experiments*. *Data are expressed relative to non-stimulated HCT astrocytes. CX3CL1 levels were normalized relative to β-actin and displayed in arbitrary units. n = 5 (number of donor cell lines per group)*. **(O)** Secreted CX3CL1 levels in HCT and SCZ astrocytes stimulated with TNF-α. *n = 10 (two replicates x number of donor cell lines per group). Data were analyzed by Two-way ANOVA, followed by Sidak's multiple comparison test. Bars represent Mean ± SEM. * $p < 0.05$, ** $p < 0.01$, *** $p < 0.001$.*

FIGURE 2: iMGs displayed a dysfunctional transcriptional profile after incubation with A_{CM} from TNF-α-stimulated SCZ astrocytes. (A) Principal component (PC) analysis of iMG samples incubated with all four distinct A_{CM} sources. (*left*) PC1 x PC2; (*middle*) PC1 x PC3; (*right*) PC2 x PC3. **(B)** Venn diagrams showing shared upregulated (*left*) and downregulated (*right*) DEGs

between iMGs exposed to A_{CM} HCT (+TNF-α), A_{CM} SCZ (N.S.) or A_{CM} SCZ (+TNF-α). **(C)** Volcano plot depicting DEGs in iMGs cultured with: (*left*) A_{CM} HCT (+TNF-α) vs A_{CM} HCT (N.S.), (*middle*) A_{CM} SCZ (N.S.) vs A_{CM} HCT (N.S.), and (*right*) A_{CM} SCZ (+TNF-α) vs A_{CM} HCT (N.S.). Upregulated and downregulated DEGs are colored in red and blue, respectively. Circles and triangles indicate genes within and out of the plot axes range, respectively. **(D)** Gene-set enrichment analysis (GSEA) plot results presenting the most relevant GO Biological Processes associated with each experimental condition. *vs means that the indicated analysis is expressed relative to iMGs + A_{CM} HCT (N.S.).* **(E)** Heatmaps indicating relative gene expression levels in iMGs after incubation with A_{CM} HCT (N.S.), A_{CM} HCT (+TNF-α), A_{CM} SCZ (N.S.) or A_{CM} SCZ (+TNF-α). Each plot indicates the top 25 non-redundant genes associated with the following GO terms: *Leukocyte Migration, Chemotaxis, Phagocytosis* and *Receptor-mediated endocytosis*. Indicated genes may belong to more than one GO term. Data are displayed as mean-centered values*. Asterisks indicate differentially expressed genes (adjusted p-value < 0.05; $|log_2$ Fold-change$|$ ≥ 0.5).*

Figure 3: Identification of putative transcription factors that regulate co-expressed gene networks associated with impaired function in iMGs exposed to A_{CM} SCZ (+TNF-α). (A) Module-trait relationships heatmap displaying the correlation between WGCNA co-expression module eigengenes and each experimental condition (i.e., iMGs + indicated A_{CM}). *Numbers in parentheses indicate adjusted p-values; above them are shown correlation values*. **(B-D)** Top 20 GO Biological Processes enriched in the *blueviolet* **(B)**, *brown* **(C)** and *darkolivegreen2* **(D)** WGCNA modules. **(E)** *In silico* master regulator analysis depicting putative transcription factors (*columns*), whose predicted target genes showed significant overlap with the indicated WGCNA modules gene sets (*rows*). *Column names in blue or red indicate master regulators exclusively found in either iMGs + A_{CM} HCT (+TNF-α) or iMGs + A_{CM} SCZ (+TNF-α), respectively, while regulons shared by at least two experimental conditions are shown in black.*

Figure 4: TNF-α-stimulated SCZ astrocytes promote a dystrophic microglial phenotype, leading to accelerated transcriptional age in iMGs. (A) iMGs' molecular phenotypes identified after exposure to the indicated A_{CM} based on the human dorsolateral prefrontal cortex microglial transcriptional signatures described by Prater *et al* (2023) (35). **(B)** Microglial-like cells signature was assessed against the CellAge database (41), whose genes are associated to either induction (*CellAge_Induces*), inhibition (*CellAge_Inhibits*) or have a context-dependent role (*CellAge_Unclear*) in promoting cellular senescence. *Only significant ($p < 0.1$) associations are colored in **(A)** and **(B)**.* **(C-H)** mRNA expression of cellular senescence markers IL-1α **(C)**, CDKN1A **(D),** CDKN2B **(E),** MKI67 **(F),** MMP12 and SERPINE1 **(H)** in iMGs cultured with A_{CM} HCT (N.S.), A_{CM} HCT (+TNF-α), A_{CM} SCZ (N.S.) or A_{CM} SCZ (+TNF-α). *n = 3 (RNA-seq replicates). Data are shown in TPM (transcripts per million reads). Data were analyzed by Two-way ANOVA, followed by Sidak's multiple comparison test. Bars represent Mean ± SEM. * $p < 0.05$, ** $p < 0.01$, *** $p < 0.001$.* **(I)** Transcriptional age gap calculated from the gene expression profile of iMGs incubated with the indicated A_{CM} and expressed relative to the mean of iMGs + A_{CM} HCT (N.S.) samples (mean was set as 0). *Data were analyzed by Two-way ANOVA, followed by Sidak's multiple comparison test. Compact-letter display (*a*,* b *and* c*) shows the statistically significant groups ($p < 0.05$).*

FIGURE 5: TNF-α-stimulated SCZ astrocytes impaired synaptoneurosomes engulfment by iMGs in a CX3CR1-independent manner. (A) Experimental design of synaptoneurosomes phagocytosis assay by iMGs after pre-treatment with AZD8797 (5 µM) and exposure to A_{CM}. *Schematic picture was drawn on Biorender.* **(B)** iMGs (bright field) engulfing CM-DiI-labeled synaptoneurosomes (red) upon incubation with A_{CM} and after pre-treatment with the CX3CR1 antagonist AZD8797. Panel depicting 16 h time-point. *Scale bar = 100 µm.* **(C)** Quantification of synaptoneurosomes uptake by iMGs incubated with A_{CM} and pre-treated with AZD8797 depicted in **(B)** and **Figure S8***.* Blue symbols: A_{CM} from HCT astrocytes; red symbols: A_{CM} from SCZ astrocytes; open symbols: A_{CM} from non-stimulated astrocytes; filled symbols: A_{CM} from TNF-α-stimulated astrocytes; circles and solid lines: vehicle

(DMSO)-treated iMGs; squares and dashed lines: AZD8797-treated iMGs. *n = 355-744 (number of cells in 4 different fields of two independent experiments). Data were analyzed by Multilevel Mixed-effects linear regression, followed by Sidak's multiple comparison test. Symbols represent Mean ± SEM. Pairwise significant comparisons are shown at the right side of the plot.* **(D-E)** Schematic representation depicting statistically significant differences depicting as reference groups vehicle-treated iMGs + ACM HCT (N.S.) **(D)** and AZD8797-treated iMGs + ACM HCT (N.S.) **(E)**, respectively.

FIGURE 6: TNF-α-stimulated HCT and SCZ astrocytes promoted similar microglial migration in a CX3CR1-dependent manner. (A) Migrated iMGs after overnight incubation with A_{CM} and pre-treatment with either vehicle (DMSO) or the CX3CR1 antagonist AZD8797 (5 µM). Nuclei were stained with Hoechst (grayscale). *Scale bar = 100 µm.* **(B)** Quantification of iMGs' migration shown in **(A)**. *n = 14 (4-5 fields per transwell x number of transwells per group). Data were normalized relative to the percentage of migrated iMGs in vehicle-treated cells cultured overnight in the presence of A_{CM} HCT (N.S.). Data were analyzed by Three-way ANOVA, followed by Sidak's multiple comparison test. Bars represent Mean ± SEM.* **(C-D)** CX3CR1 relative protein levels measured in the plasma membrane **(C)** and in the whole cell **(D)** in iMGs incubated with A_{CM} for 24 h. *n = 9-10 (number of replicates in two independent experiments). Data were analyzed by Two-way ANOVA, followed by Sidak's multiple comparison test. Bars represent Mean ± SEM. * $p < 0.05$, ** $p < 0.01$, *** $p < 0.001$.*

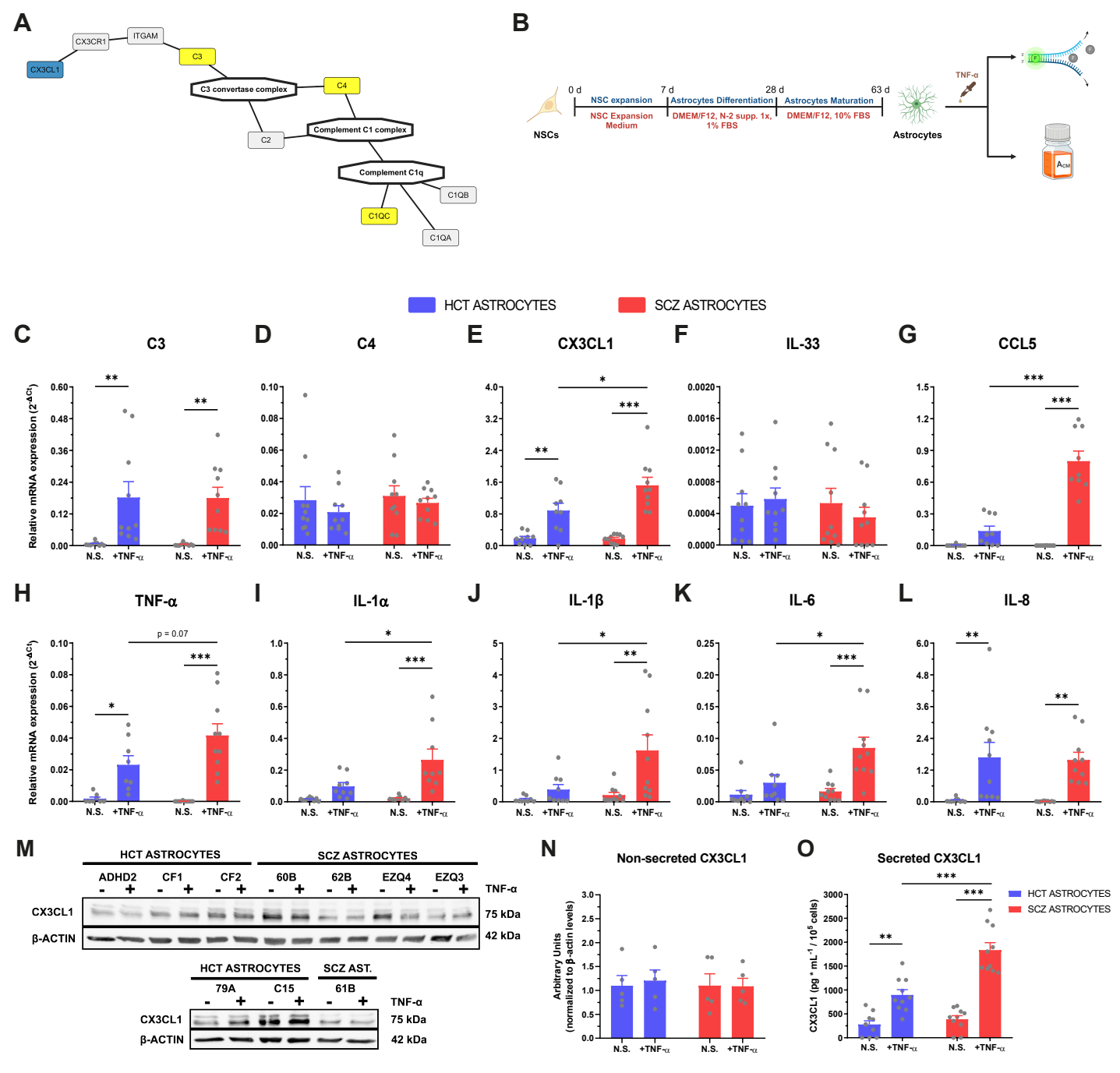
A
CX3CL1
CX3CR1
ITGAM
C3
C3 convertase complex
C4
C2
Complement C1 complex
Complement C1q
C1QB
C1QC
C1QA
B
NSCs
0 d
NSC expansion
NSC Expansion Medium
7 d
Astrocytes Differentiation
DMEM/F12, N-2 supp. 1x, 1% FBS
28 d
Astrocytes Maturation
DMEM/F12, 10% FBS
63 d
Astrocytes
TNF-α
ACM
HCT ASTROCYTES
SCZ ASTROCYTES
C
C3
D
C4
E
CX3CL1
F
IL-33
G
CCL5
Relative mRNA expression (2^-ΔCt)
N.S.
+TNF-α
H
TNF-α
p = 0.07
I
IL-1α
J
IL-1β
K
IL-6
L
IL-8
M
HCT ASTROCYTES
SCZ ASTROCYTES
ADHD2
CF1
CF2
60B
62B
EZQ4
EZQ3
TNF-α
CX3CL1
β-ACTIN
75 kDa
42 kDa
HCT ASTROCYTES
SCZ AST.
79A
C15
61B
N
Non-secreted CX3CL1
Arbitrary Units (normalized to β-actin levels)
O
Secreted CX3CL1
CX3CL1 (pg * mL^-1 / 10^6 cells)
HCT ASTROCYTES
SCZ ASTROCYTES

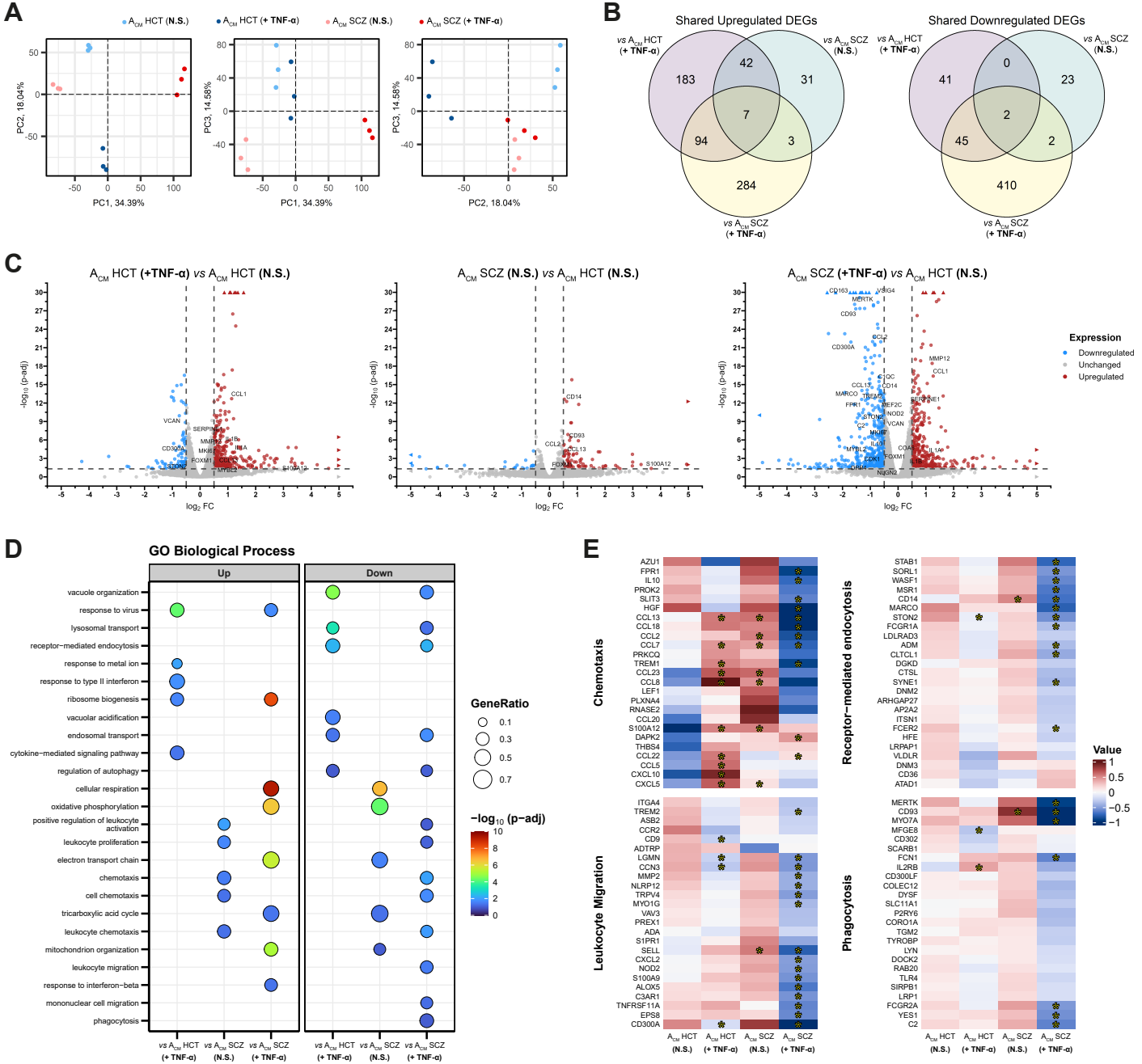
A
A_CM HCT (N.S.)
A_CM HCT (+ TNF-α)
A_CM SCZ (N.S.)
A_CM SCZ (+ TNF-α)
PC2, 18.04%
PC3, 14.58%
PC1, 34.39%
B
Shared Upregulated DEGs
Shared Downregulated DEGs
vs A_CM HCT (+ TNF-α)
vs A_CM SCZ (N.S.)
vs A_CM SCZ (+ TNF-α)
183
42
31
7
94
3
284
41
0
23
2
45
2
410
C
A_CM HCT (+TNF-α) vs A_CM HCT (N.S.)
A_CM SCZ (N.S.) vs A_CM HCT (N.S.)
A_CM SCZ (+TNF-α) vs A_CM HCT (N.S.)
-log10 (p-adj)
log2 FC
Expression
Downregulated
Unchanged
Upregulated
D
GO Biological Process
Up
Down
vacuole organization
response to virus
lysosomal transport
receptor−mediated endocytosis
response to metal ion
response to type II interferon
ribosome biogenesis
vacuolar acidification
endosomal transport
cytokine−mediated signaling pathway
regulation of autophagy
cellular respiration
oxidative phosphorylation
positive regulation of leukocyte activation
leukocyte proliferation
electron transport chain
chemotaxis
cell chemotaxis
tricarboxylic acid cycle
leukocyte chemotaxis
mitochondrion organization
leukocyte migration
response to interferon−beta
mononuclear cell migration
phagocytosis
GeneRatio
0.1
0.3
0.5
0.7
−log10 (p−adj)
10
8
6
4
2
0
E
Chemotaxis
Leukocyte Migration
Receptor−mediated endocytosis
Phagocytosis
Value
1
0.5
0
−0.5
−1
A_CM HCT (N.S.)
A_CM HCT (+ TNF-α)
A_CM SCZ (N.S.)
A_CM SCZ (+ TNF-α)

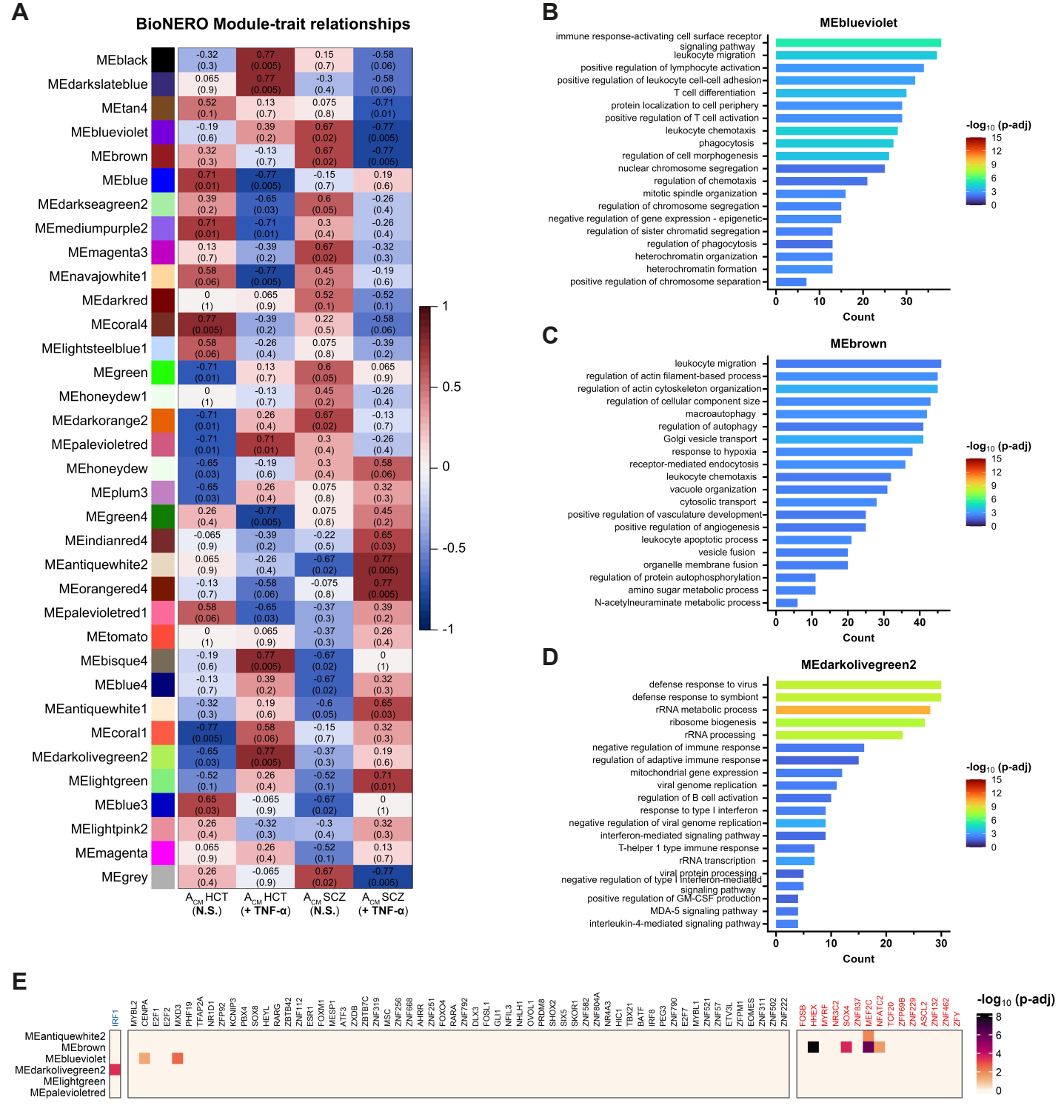
A
BioNERO Module-trait relationships
MEblack -0.32 (0.3) 0.77 (0.005) 0.15 (0.7) -0.58 (0.06)
MEdarkslateblue 0.065 (0.9) 0.77 (0.005) -0.3 (0.4) -0.58 (0.06)
MEtan4 0.52 (0.1) 0.13 (0.7) 0.075 (0.8) -0.71 (0.01)
MEblueviolet -0.19 (0.6) 0.39 (0.2) 0.67 (0.02) -0.77 (0.005)
MEbrown 0.32 (0.3) -0.13 (0.7) 0.67 (0.02) -0.77 (0.005)
MEblue 0.71 (0.01) -0.77 (0.005) -0.15 (0.7) 0.19 (0.6)
MEdarkseagreen2 0.39 (0.2) -0.65 (0.03) 0.6 (0.05) -0.26 (0.4)
MEmediumpurple2 0.71 (0.01) -0.71 (0.01) 0.3 (0.4) -0.26 (0.4)
MEmagenta3 0.13 (0.7) -0.39 (0.2) 0.67 (0.02) -0.32 (0.3)
MEnavajowhite1 0.58 (0.06) -0.77 (0.005) 0.45 (0.2) -0.19 (0.6)
MEdarkred 0 (1) 0.065 (0.9) 0.52 (0.1) -0.52 (0.1)
MEcoral4 0.77 (0.005) -0.39 (0.2) 0.22 (0.5) -0.58 (0.06)
MElightsteelblue1 0.58 (0.06) -0.26 (0.4) 0.075 (0.8) -0.39 (0.2)
MEgreen -0.71 (0.01) 0.13 (0.7) 0.6 (0.05) 0.065 (0.9)
MEhoneydew1 0 (1) -0.13 (0.7) 0.45 (0.2) -0.26 (0.4)
MEdarkorange2 -0.71 (0.01) 0.26 (0.4) 0.67 (0.02) -0.13 (0.7)
MEpalevioletred -0.71 (0.01) 0.71 (0.01) 0.3 (0.4) -0.26 (0.4)
MEhoneydew -0.65 (0.03) -0.19 (0.6) 0.3 (0.4) 0.58 (0.06)
MEplum3 -0.65 (0.03) 0.26 (0.4) 0.075 (0.8) 0.32 (0.3)
MEgreen4 0.26 (0.4) -0.77 (0.005) 0.075 (0.8) 0.45 (0.2)
MEindianred4 -0.065 (0.9) -0.39 (0.2) -0.22 (0.5) 0.65 (0.03)
MEantiquewhite2 0.065 (0.9) -0.26 (0.4) -0.67 (0.02) 0.77 (0.005)
MEorangered4 -0.13 (0.7) -0.58 (0.06) -0.075 (0.8) 0.77 (0.005)
MEpalevioletred1 0.58 (0.06) -0.65 (0.03) -0.37 (0.3) 0.39 (0.2)
MEtomato 0 (1) 0.065 (0.9) -0.37 (0.3) 0.26 (0.4)
MEbisque4 -0.19 (0.6) 0.77 (0.005) -0.67 (0.02) 0 (1)
MEblue4 -0.13 (0.7) 0.39 (0.2) -0.67 (0.02) 0.32 (0.3)
MEantiquewhite1 -0.32 (0.3) 0.19 (0.6) -0.6 (0.05) 0.65 (0.03)
MEcoral1 -0.77 (0.005) 0.58 (0.06) -0.15 (0.7) 0.32 (0.3)
MEdarkolivegreen2 -0.65 (0.03) 0.77 (0.005) -0.37 (0.3) 0.19 (0.6)
MElightgreen -0.52 (0.1) 0.26 (0.4) -0.52 (0.1) 0.71 (0.01)
MEblue3 0.65 (0.03) -0.065 (0.9) -0.67 (0.02) 0 (1)
MElightpink2 0.26 (0.4) -0.32 (0.3) -0.3 (0.4) 0.32 (0.3)
MEmagenta 0.065 (0.9) 0.26 (0.4) -0.52 (0.1) 0.13 (0.7)
MEgrey 0.26 (0.4) -0.065 (0.9) 0.67 (0.02) -0.77 (0.005)
A_CM HCT (N.S.)
A_CM HCT (+ TNF-α)
A_CM SCZ (N.S.)
A_CM SCZ (+ TNF-α)
1
0.5
0
-0.5
-1
B
MEblueviolet
immune response-activating cell surface receptor signaling pathway
leukocyte migration
positive regulation of lymphocyte activation
positive regulation of leukocyte cell-cell adhesion
T cell differentiation
protein localization to cell periphery
positive regulation of T cell activation
leukocyte chemotaxis
phagocytosis
regulation of cell morphogenesis
nuclear chromosome segregation
regulation of chemotaxis
mitotic spindle organization
regulation of chromosome segregation
negative regulation of gene expression - epigenetic
regulation of sister chromatid segregation
regulation of phagocytosis
heterochromatin organization
heterochromatin formation
positive regulation of chromosome separation
0 10 20 30
Count
-log10 (p-adj)
15 12 9 6 3 0
C
MEbrown
leukocyte migration
regulation of actin filament-based process
regulation of actin cytoskeleton organization
regulation of cellular component size
macroautophagy
regulation of autophagy
Golgi vesicle transport
response to hypoxia
receptor-mediated endocytosis
leukocyte chemotaxis
vacuole organization
cytosolic transport
positive regulation of vasculature development
positive regulation of angiogenesis
leukocyte apoptotic process
vesicle fusion
organelle membrane fusion
regulation of protein autophosphorylation
amino sugar metabolic process
N-acetylneuraminate metabolic process
0 10 20 30 40
Count
-log10 (p-adj)
15 12 9 6 3 0
D
MEdarkolivegreen2
defense response to virus
defense response to symbiont
rRNA metabolic process
ribosome biogenesis
rRNA processing
negative regulation of immune response
regulation of adaptive immune response
mitochondrial gene expression
viral genome replication
regulation of B cell activation
response to type I interferon
negative regulation of viral genome replication
interferon-mediated signaling pathway
T-helper 1 type immune response
rRNA transcription
viral protein processing
negative regulation of type I interferon-mediated signaling pathway
positive regulation of GM-CSF production
MDA-5 signaling pathway
interleukin-4-mediated signaling pathway
0 10 20 30
Count
-log10 (p-adj)
15 12 9 6 3 0
E
IRF1
MYBL2 CENPA E2F1 E2F2 MXD3 PHF19 TFAP2A NR1D1 ZFP92 KCNIP3 PBX4 SOX8 HEYL RARG ZBTB42 ZNF112 ESR1 FOXM1 MESP1 ATF3 ZXDB ZBTB7C ZNF319 MSC ZNF256 ZNF668 AHRR ZNF251 FOXO4 RARA ZNF792 DLX3 FOSL1 GLI1 NFIL3 NHLH1 OVOL1 PRDM8 SHOX2 SIX5 SKOR1 ZNF582 ZNF804A NR4A3 HIC1 TBX21 BATF IRF8 PEG3 ZNF790 E2F7 MYBL1 ZNF521 ZNF57 ETV3L ZFPM1 EOMES ZNF311 ZNF502 ZNF222
FOSB HHEX MYRF NR3C2 SOX4 ZNF837 MEF2C NFATC2 TCF20 ZFP69B ZNF229 ASCL2 ZNF132 ZNF462 ZFY
MEantiquewhite2
MEbrown
MEblueviolet
MEdarkolivegreen2
MElightgreen
MEpalevioletred
-log10 (p-adj)
8 6 4 2 0

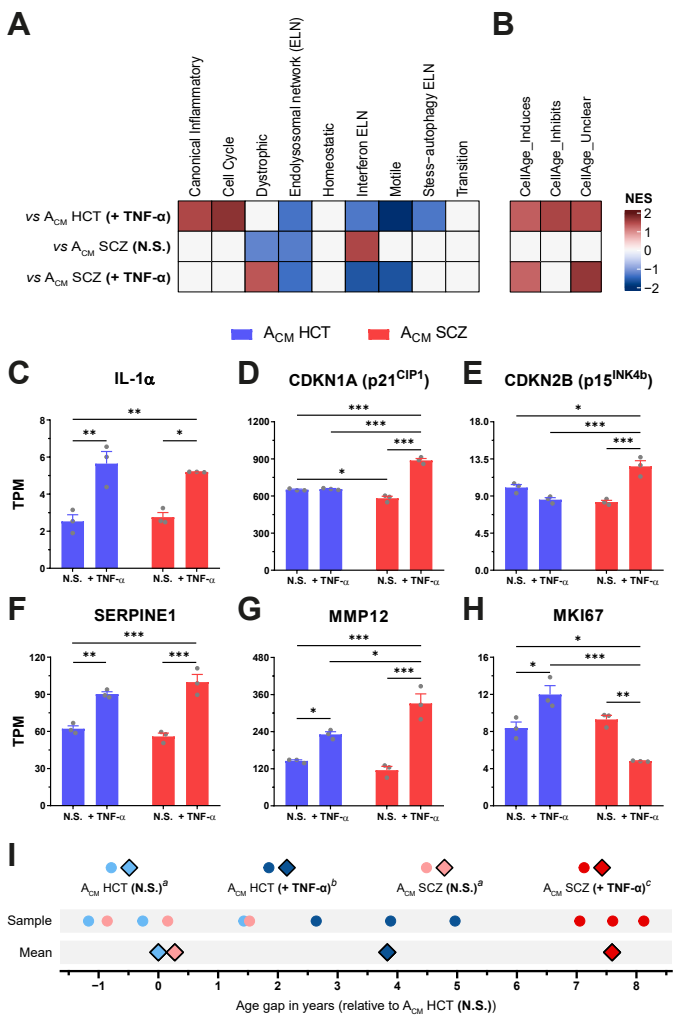
A
Canonical Inflammatory
Cell Cycle
Dystrophic
Endolysosomal network (ELN)
Homeostatic
Interferon ELN
Motile
Stess-autophagy ELN
Transition
vs A_CM HCT (+ TNF-α)
vs A_CM SCZ (N.S.)
vs A_CM SCZ (+ TNF-α)
B
CellAge_Induces
CellAge_Inhibits
CellAge_Unclear
NES
2
1
0
−1
−2
A_CM HCT
A_CM SCZ
C
IL-1α
D
CDKN1A (p21^CIP1)
E
CDKN2B (p15^INK4b)
F
SERPINE1
G
MMP12
H
MKI67
TPM
N.S.
+ TNF-α
I
A_CM HCT (N.S.)^a
A_CM HCT (+ TNF-α)^b
A_CM SCZ (N.S.)^a
A_CM SCZ (+ TNF-α)^c
Sample
Mean
Age gap in years (relative to A_CM HCT (N.S.))

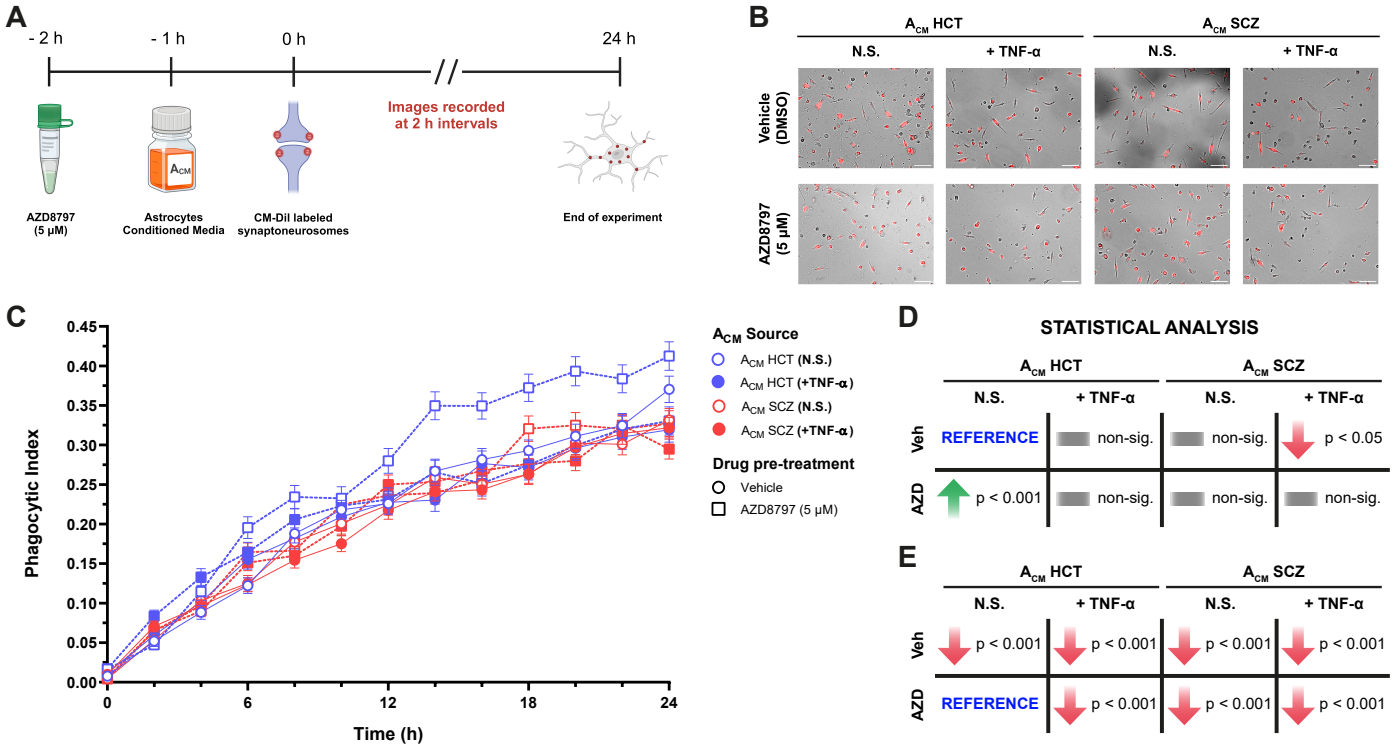
A
- 2 h
- 1 h
0 h
24 h
Images recorded at 2 h intervals
AZD8797 (5 μM)
Astrocytes Conditioned Media
CM-DiI labeled synaptoneurosomes
End of experiment
B
A_CM HCT
A_CM SCZ
N.S.
+ TNF-α
Vehicle (DMSO)
AZD8797 (5 μM)
C
Phagocytic Index
Time (h)
A_CM Source
A_CM HCT (N.S.)
A_CM HCT (+TNF-α)
A_CM SCZ (N.S.)
A_CM SCZ (+TNF-α)
Drug pre-treatment
Vehicle
AZD8797 (5 μM)
D
STATISTICAL ANALYSIS
Veh
AZD
REFERENCE
non-sig.
p < 0.05
p < 0.001
E
REFERENCE

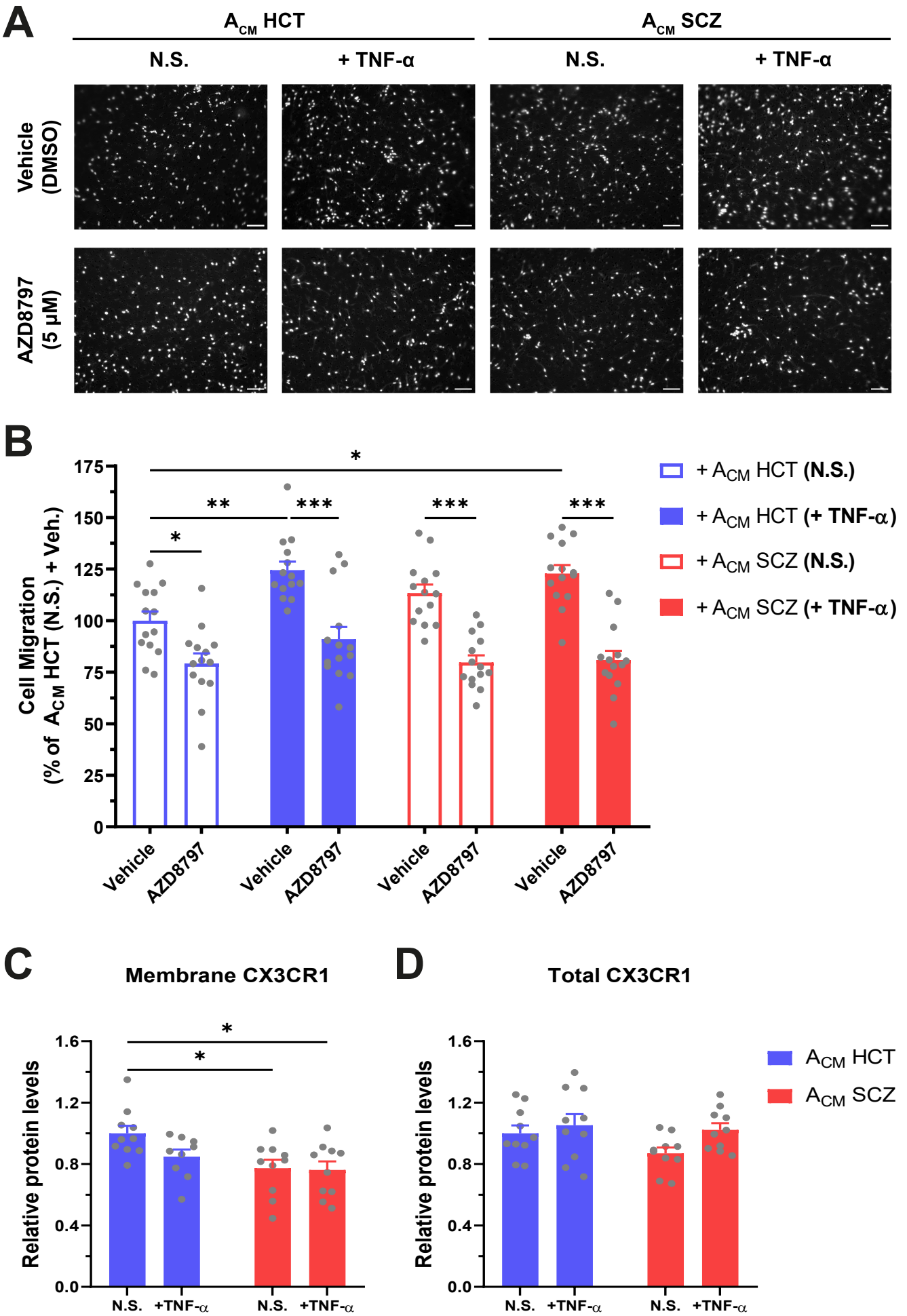
A
A_{CM} HCT
A_{CM} SCZ
N.S.
+ TNF-α
N.S.
+ TNF-α
Vehicle (DMSO)
AZD8797 (5 μM)
B
Cell Migration (% of A_{CM} HCT (N.S.) + Veh.)
175
150
125
100
75
50
25
0
*
**
***
***
***
*
Vehicle
AZD8797
Vehicle
AZD8797
Vehicle
AZD8797
Vehicle
AZD8797
+ A_{CM} HCT (N.S.)
+ A_{CM} HCT (+ TNF-α)
+ A_{CM} SCZ (N.S.)
+ A_{CM} SCZ (+ TNF-α)
C
Membrane CX3CR1
Relative protein levels
1.6
1.2
0.8
0.4
0.0
*
*
N.S.
+TNF-α
N.S.
+TNF-α
D
Total CX3CR1
Relative protein levels
1.6
1.2
0.8
0.4
0.0
N.S.
+TNF-α
N.S.
+TNF-α
A_{CM} HCT
A_{CM} SCZ